The Topography of the Central and Peripheral Cornea

Scott A. Read, Michael J. Collins, Leo G. Carney, and Ross J. Franklin

Purpose. To investigate the topography of the central and peripheral cornea in a group of young adult subjects with a range of normal refractive errors.

Methods. Corneal topography data were acquired for 100 young adult subjects by a method that allows central and peripheral maps to be combined to produce one large, extended corneal topography map. This computer-based method involves matching the common topographical features in the overlapping maps. Corneal height, axial radius of curvature, and axial power data were analyzed. The corneal height data were also fit with Zernike polynomials.

Results. Conic fitting to the corneal height data revealed the average apical radius (*R*o) was 7.77 ± 0.2-mm and asphericity (*Q*) was −0.19 ± 0.1 for a 6-mm corneal diameter. The conic fit parameters were both found to change significantly for increasing corneal diameters. For a 10-mm corneal diameter, *R*o was 7.72 ± 0.2 mm and *Q* was −0.36 ± 0.1. A slight but significant meridional variation was found in *Q*, with the steepest principal corneal meridian found to flatten at a slightly greater rate than the flattest meridian. The RMS fit error for the conic section was found to increase markedly for larger corneal diameters. Higher-order polynomial fits were needed to fit the peripheral corneal data adequately. Analysis of the axial power data revealed highly significant changes occurring in the corneal best-fit spherocylinder with increasing distance from the corneal center. The peripheral cornea was found to become significantly flatter and to decrease slightly in its toricity. Individual subjects exhibited a range of different patterns of central and peripheral corneal topography. Several of the higher order corneal surface Zernike coefficients were found to change significantly with increasing corneal diameter.

Conclusions. Highly significant changes occur in the shape of the cornea in the periphery. On average, the peripheral cornea becomes significantly flatter and slightly less astigmatic than the central cornea. A conic section is a poor estimator of the peripheral cornea. (*Invest Ophthalmol Vis Sci.* 2006;47:1404–1415) DOI:10.1167/iovs.05-1181

The advent of computer-assisted videokeratoscopes has greatly improved our understanding of the cornea's shape and its optics. The detailed information provided by these instruments is used in the diagnosis of corneal ectatic disorders such as keratoconus,[1] in rigid and soft contact lens fitting,[2–4] in the screening of refractive surgery candidates,[5,6] and for customized refractive surgery corrections.[7–10]

A simple and commonly used method to describe corneal shape quantitatively is as a conic section, defined by the apical radius (*R*o) and the asphericity parameter (*Q*), which describes the type of conicoid that best fits the corneal shape (i.e., the degree to which the surface departs from a sphere) where $Q = 0$ describes a sphere, $Q > 0$ describes an oblate or steepening ellipse, and $-1 < Q < 0$ describes a prolate, or flattening, ellipse.

Several studies have derived the average *R*o and *Q* for a normal adult population.[11–15] These studies have produced average *R*o ranging from 7.68 to 7.85 and average *Q* ranging from −0.33 to −0.18 (i.e., nearly all subjects exhibit corneas with a prolate elliptical shape). Although the average results across these studies have been relatively consistent, most investigators note that large variations in corneal shape exist between normal subjects. Recently, more complex quantitative descriptors of shape such as Fourier series analysis[16] and Zernike polynomials[17,18] have been used to describe the shape of the cornea.

Most studies of corneal shape have investigated the central 6 mm of the cornea. Although data from the central cornea are obviously the most important for vision, this represents only approximately one fourth of the cornea's total surface area. Information from the peripheral cornea is particularly important in the design and fitting of contact lenses. The area of the cornea measured by videokeratoscopes is much larger than that of the traditional keratometer. For videokeratoscopes based on the Placido disc principle, corneal coverage is limited by the fact that the instrument is based on specular reflection from the corneal surface and further limited by obscuration of the ring image by the subjects' nose, brow, and eyelashes.[19] Corneal coverage with Placido-based videokeratoscopes is improved by using a small measurement cone, as obscuration by the nose and brow is avoided. Videokeratoscopes based on other principles (such as slit scanning and raster stereography techniques) have the potential to measure larger corneal areas than Placido-based systems,[20] although they are still limited by interference from the eyelids and eyelashes. However, these other techniques have generally not proved to be as precise or accurate in their measurements as small cone Placido-based systems.[21,22]

There have been relatively few studies investigating the shape of the peripheral cornea, outside the central 6-mm diameter. Mandell[23] used offset fixation points in a videokeratoscope to measure peripheral corneal topography in 11 subjects and found that for peripheral measurements, an ellipse was a poor descriptor of cornea shape, due to increased flattening of the corneal surface in the periphery. An average tangential radius of 11.29 ±1.82 mm was found at 4.5 mm from corneal center for the 11 subjects tested. Reddy et al.[3] classified subjects' corneal astigmatism based on central and peripheral corneal topography data.

We have recently developed a technique that allows measurement of the peripheral cornea and the subsequent combination of central and peripheral corneal topography data to provide a total corneal topography map.[24] Using this technique, we measured the total corneal topography of the right eyes of 100 subjects. The purpose of this study was to provide normative information regarding the shape of the total cornea

From the Contact Lens and Visual Optics Laboratory, School of Optometry, Queensland University of Technology, Brisbane, Queensland, Australia.

Submitted for publication September 3, 2005; revised November 2, 2005; accepted February 15, 2006.

Disclosure: **S.A. Read**, None; **M.J. Collins**, None; **L.G. Carney**, None; **R.J. Franklin**, None

The publication costs of this article were defrayed in part by page charge payment. This article must therefore be marked "*advertisement*" in accordance with 18 U.S.C. §1734 solely to indicate this fact.

Corresponding author: Scott A. Read, Contact Lens and Visual Optics Laboratory, School of Optometry, Queensland University of Technology, Room B547, O Block, Victoria Park Road, Kelvin Grove 4059, Brisbane, Queensland, Australia; sa.read@qut.edu.au.

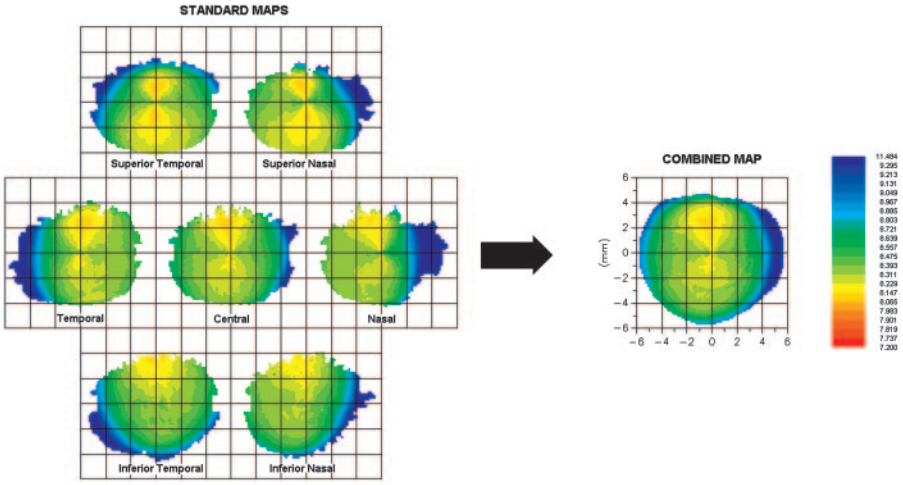

FIGURE 1. Example of central and peripheral corneal data and combined data map (axial curvature maps are shown). The map correlation process attempts to find the point in each of the peripheral maps that corresponds to the vertex normal of the central map. Each peripheral map is then rotated and combined with the central map to produce the combined corneal topography map (*right*).

for a large population of young, healthy, adult subjects with a range of normal refractive errors.

METHODS

Subjects and Procedure

Corneal topography maps were acquired for the right eyes of 100 young adult subjects. All subjects had normal ocular health with no history of ocular surgery, trauma, or corneal disease. No full-time soft contact lens (SCL) or rigid gas-permeable (RGP) contact lens wearers were included in the study. Nine parttime SCL wearers were included, but were instructed not to wear contact lenses on the day of testing. Approval from the university human research ethics committee was obtained before commencement of the study, and informed consent was obtained from all the subjects. All subjects were treated in accordance with the tenets of the Declaration of Helsinki.

Of the 100 subjects participating, eight subjects were excluded from subsequent analyses due to poor correlation between central and peripheral corneal topography maps (the criteria for subject exclusion due to poor map correlation is described later). This left 92 subjects in the final data analysis. The subjects' ages ranged from 18 to 35 years, with a mean age of 24 years. Of the 92 subjects, 54 were women. The subjects exhibited a range of refractive error, with the group mean best sphere refractive error being -1.1 ± 1.8 D (range, $+0.63$ D to -8.13 D) and group mean astigmatic refractive error being -0.32 ± 0.6 D (range, 0 D to -2.75 D). So that we could rule out any significant anterior eye or tear film abnormalities, each subject underwent a preliminary slit lamp examination.

All corneal topography measurements were taken with a videokeratoscope (model E300 videokeratoscope; Medmont Pty. Ltd., Victoria, Australia). The E300 is based on the Placido disc principle and has been shown to have a high degree of accuracy and precision for measuring inanimate test objects.[21] Tang et al.[21] found the E300 to exhibit a mean height error of 2 μm for measuring spherical and aspheric test surfaces. This instrument has also exhibited highly repeatable results for measurements on corneas in vivo.[22] Cho et al.[22] found that two repeated measurements were required with the instrument to ensure a precision in corneal elevation data of 2 μm. The videokeratoscope has a sophisticated range-finding device that determines the distance from the corneal apex to the instrument's camera and automatically captures the videokeratoscopic image only when good focus and alignment of the eye are attained. To reduce the effects of any diurnal variation in corneal topography, all measurements were taken in the morning.[25] As prior visual tasks may also affect corneal topography, subjects were also asked to refrain from performing significant close work immediately before testing.[25,26]

The procedure used for measuring the total corneal topography has been described in detail.[24] The corneal topography of one eye is measured while the subject views an external-fixation target positioned 1.5 m away from the videokeratoscope with the fellow eye (through the use of a mirror). The external-fixation target has a central target and six peripheral targets in different peripheral angles of gaze (at 0°, 60°, 120°, 180°, 240°, and 300° and approximately 30 cm from the central target). Three videokeratoscope images are captured with the subject fixating on the instrument's internal central fixation target. The subject is then instructed to fixate on the external target with the fellow eye, and videokeratoscope images are captured with the subject looking at each of the six peripheral fixation targets in turn. A total of four videokeratoscope images are captured for each of the six peripheral directions of gaze (i.e., 3 central images and 24 peripheral images are captured).

The corneal height data for each of the videokeratoscope images is exported from the instrument and is analyzed with custom-written software[24] that examines the correlation between central and peripheral corneal topography data. The purpose of this process is to find the point in the peripheral map corresponding to the center of the central topography map (the vertex normal). Essentially, it locates the point on the peripheral map (defined by the radial distance, azimuthal angle, and degree of cyclorotation from the center of the peripheral map) where the sum of squares of differences in the overlapping portions of the central and peripheral corneal topography maps is minimized.

The central topography map is correlated with each of the four peripheral maps in one direction of peripheral gaze, and the peripheral map that gives the best correlation (i.e., the smallest sum of squares difference) with the central map is chosen as the best peripheral map for that direction of gaze. This procedure is repeated for each of the six directions of peripheral gaze. The one central map and six peripheral maps are then chosen that give the overall smallest sum of squares of differences between central and peripheral corneal topography data.

After this map correlation process, the central and peripheral maps are combined. The point of best correlation in each peripheral map is rotated to make this point the common vertex normal, and the peripheral maps are then combined with the central map. In the combined map, the central 6 mm of the central map is preserved, and the peripheral data are added past this point. The combined map is output in the same format as the standard Medmont height map except that the combined map has 46 rings of data in 300 semimeridians (the standard Medmont height map has 32 rings of data). Combined axial radius of curvature maps were also calculated based on the combined corneal height maps. Figure 1 shows an example of central and peripheral corneal axial radius of curvature maps and a combined data map for one subject.

To assess the accuracy of this process, Franklin et al.[24] compared the original central map data with the rotated peripheral map data. Data from a conic test surface showed a less than 0.5 μm difference between central and rotated peripheral data, and data from a real cornea showed errors between the central and rotated peripheral maps of less than 1 μm across the central 7 mm of data.

If central and peripheral maps correlate well, then the combined map exhibits a smooth transition between central data (the central 6-mm diameter) and peripheral data (outside of the central 6-mm diameter). A feature of combined maps with poor correlation is a large change at the junction between the central and peripheral corneal data.

To determine what would be an unacceptable difference in axial curvature at the junction between the central and peripheral data, every semimeridian of axial curvature data from every subject's standard central map was analyzed and a second-order polynomial function fit to a small region of data just inside 3 mm from the corneal center for each map. The difference between the actual axial radius and the axial radius predicted by the polynomial fit was then calculated for the point just outside 3 mm from center for each semimeridian. The average and SD of the difference between actual and predicted axial radius was found to be 0.04 ± 0.07 mm with an outer 95% confidence interval of 0.18 mm.

The combined central and peripheral axial radius of curvature maps were analyzed in a similar fashion. A polynomial function was fit to the final five central map data points just inside 3 mm from corneal center, and the predicted data were then compared to the first two peripheral map data points at 3.13 and 3.26 mm from corneal center. Any maps showing a difference between actual and predicted data of greater than ±0.2 mm in more than 40 semimeridians at the junction between central and peripheral data was considered to have a poor correlation (one poorly correlated peripheral map would be expected to result in an abrupt boundary change in 50 semimeridians). Of the 100 subjects who had corneal topography measurements taken, 8 were excluded due to poor correlation between central and peripheral topography data.

It is possible that changes in extraocular muscle tension (as occurs in our protocol for capturing the peripheral topography data) may cause changes in corneal topography.[27–29] A control experiment was performed to investigate whether the eye movements (and subsequent changes in extraocular muscle tension) used in our protocol to capture the peripheral corneal topography maps had an effect on the peripheral corneal topography data. Topography maps of the temporal corneal periphery were taken for two subjects, first by moving the videokeratoscope camera (i.e., no eye movements used) and second by changing fixation (i.e., eye movements used). The peripheral corneal topography data from the two conditions was then compared. No significant difference was found between the peripheral corneal data with or without eye movement. We concluded from this, that the alteration of extraocular muscle tension associated with the change in fixation in our peripheral map capturing protocol (approximately 11°) was not enough to cause significant changes in the peripheral corneal topography data.

The center of standard corneal topography maps is located at a point where the optical axis of the videokeratoscope is perpendicular to the cornea, known as the vertex normal.[30] The position of the vertex normal relative to the geometric center of the cornea is known to differ from person to person.[31] Therefore to have each subject's corneal topography map centered to a common reference point, we rotated each combined map to the corneal geometric center. The best central videokeratoscope image (as determined through the map correlation process) for each subject was analyzed to determine the position of the corneal geometric center using customized computer software that locates the corneal limbus in the videokeratoscope image.[32]

Analysis

We calculated the average size of the topography maps in the vertical and horizontal dimensions for both standard (central fixation) and combined corneal topography, by finding the shortest complete semimeridian of data within five meridians (6°) of the horizontal (temporal and nasal) and vertical (superior and inferior) directions. The shortest semimeridians in the temporal and nasal direction were combined, and the shortest semimeridians in the superior and inferior direction were also combined. This provided an estimate of the minimum horizontal and vertical map diameters for both the standard topography and the combined topography maps. Individual subject data were combined to calculate the group mean map size for each technique.

Each subject's corneal height data were averaged across all semimeridians, and the average *R*o and *Q* were calculated based on Baker's equation for conic sections: $y^2 = 2Rox - px^2$, where y is the distance from corneal center and x is the corneal height.[33] A linear in parameters least squares fitting was performed to calculate the *R*o and p for the averaged semimeridian data. The asphericity parameter Q is related to p by the equation $Q = p - 1$. *R*o and Q were calculated for 6-, 8-, 9-, and 10-mm corneal diameters. For this average across all semimeridians, only subjects with at least 200 semimeridians of complete data were included in the analysis. Any missing data (even in the combined maps) tend to be in the superior semimeridians due to interruptions from the brow and eyelashes; therefore, the larger-diameter analyses will be slightly biased toward the horizontal regions. We would expect this bias to have only a slight effect and only on the 9- and 10-mm diameter data. The root mean square (RMS) fit error was also calculated for each corneal diameter. A repeated-measures analysis of variance (ANOVA) with one within-subject factor (corneal diameter) was used to investigate whether *R*o and Q changed significantly for the different corneal diameters tested.

The conic fitting was also performed for the steepest and flattest meridians of corneal data for each subject. The steepest and flattest meridians were calculated based on the best fit spherocylinder to the corneal axial power for an 8-mm corneal diameter. The meridian of data corresponding with the corneal cylinder axis and the two adjacent meridians on either side were averaged to provide the corneal data along the flattest corneal meridian. The same procedure was performed for the steepest meridian data. The best fitting *R*o and Q were then calculated for each meridian for each subject. To investigate meridional variations in *R*o and Q, repeated-measures ANOVA was performed with two within-subject factors (corneal diameter and corneal meridian).

Franklin et al.[24] showed that for larger corneal diameters, a polynomial function fit corneal height data better than a conic fit. They found that a fourth-order polynomial was needed to fit 7-mm diameter data and that for a 10.7-mm diameter a ninth-order polynomial fit was necessary. The average corneal height data were also therefore fit with a polynomial function of the form $x = Ay + By^2 + Cy^3 + Dy^4 \ldots$ and so on (where x is the corneal height and y is the distance from corneal center). For each subject, the third- through to the ninth-order polynomial functions were all fit to the corneal height data for 6-, 8-, 9-, and 10-mm diameters. The RMS fit error was also calculated for each of the polynomial orders and for each corneal diameter.

For each subject, axial power maps were calculated based on the combined corneal height data. The axial power data for each subject were analyzed to calculate the best fit corneal spherocylinder using the method of Maloney et al.[34] We found these fitting routines to be highly sensitive to any missing data points, therefore only subjects with 300 complete semimeridians of axial power data to the edge of the outer diameter were included in each of the analyses. The best fit spherocylinder data for each subject was converted into the power vectors **M** (best sphere), **J0** (astigmatism 90°/180°) and **J45** (astigmatism 45°/135°),[35] to allow the group mean and SD to be calculated. The best fit corneal spherocylinder was calculated for corneal diameters of 6, 7, 8, and 9 mm. To investigate for significant changes in the corneal sphero-

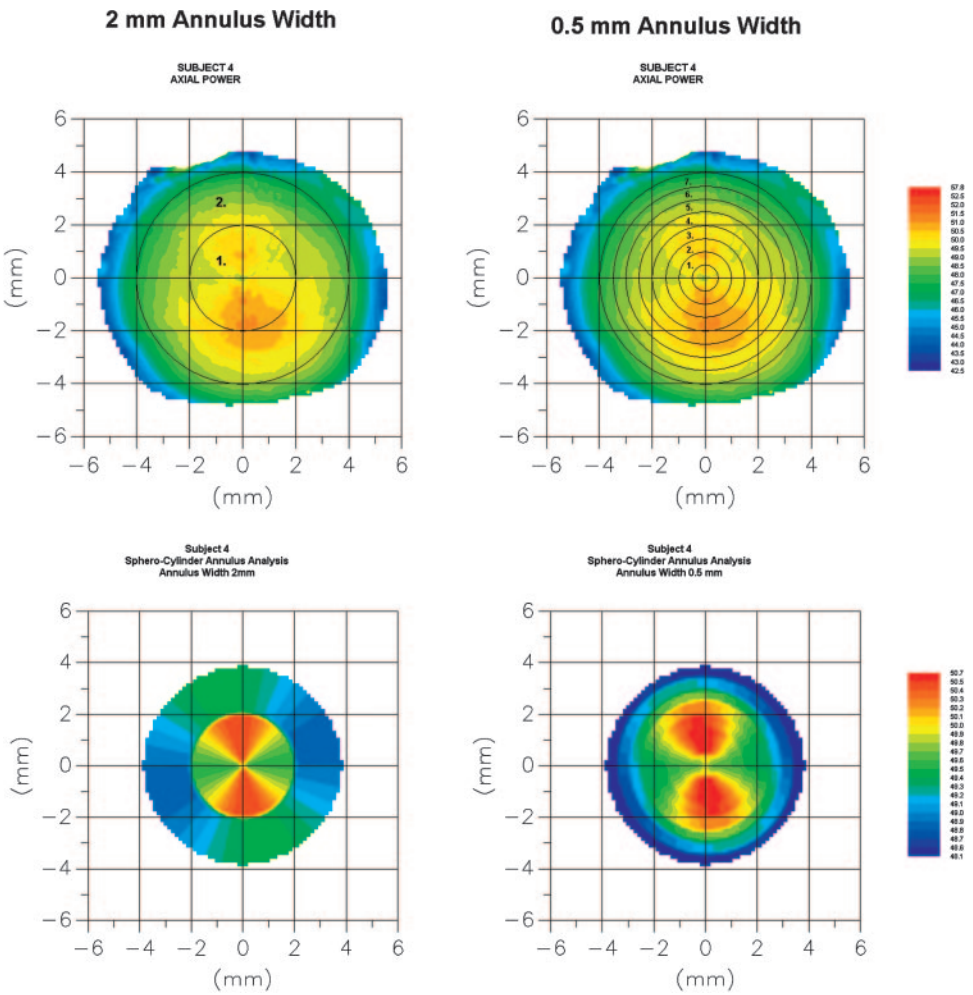

FIGURE 2. Illustration of the annulus spherocylinder analysis method used for examining the change in the corneal spherocylinder in the peripheral cornea. The best-fit spherocylinder is calculated for annuli 1 and 2 for the 2-mm width analysis (*top left*) and is calculated in annuli 1 to 7 for the 0.5-mm width analysis (*top right*). *Bottom*: the spherocylinder for each of the annuli.

cylinder with increasing diameter, a repeated-measures ANOVA was used with one within-subject factor (corneal diameter).

Changes in the corneal spherocylinder with increasing corneal diameter give some indication of variations in the peripheral cornea. However, the large-diameter corneal spherocylinder fits contain data from both the peripheral and the central cornea. Therefore some changes in the peripheral cornea may be somewhat masked by data from the central cornea. To overcome this, and to analyze further the peripheral cornea, we broke the cornea down into concentric annuli of data. This analysis has the advantage that the data in each annulus

TABLE 1. Average Conic Fit and Polynomial Fit Data from the Corneal Height Data Averaged across All Meridians

	Corneal Diameter			
	6 mm (n = 92)	**8 mm (n = 92)**	**9 mm (n = 92)**	**10 mm (n = 84)**
Conic fit				
Ro	7.77 ± 0.2	7.76 ± 0.2	7.73 ± 0.2	7.72 ± 0.2
Q	−0.19 ± 0.1	−0.23 ± 0.1	−0.30 ± 0.1	−0.36 ± 0.1
RMS fit error (μm)	0.79 ± 0.4	4.19 ± 4.4	11.66 ± 7.9	21.18 ± 11.1
Polynomial fit ($x = Ay + By^2 + Cy^3 \ldots$)				
A	−8.815E−05	−2.598E−04	−1.266E−04	−7.276E−06
B	6.467E−02	6.518E−02	6.469E−02	6.381E−02
C	−1.982E−04	−6.910E−04	−8.062E−05	1.812E−03
D	2.760E−04	4.659E−04	1.280E−04	−2.235E−03
E		−2.549E−05	6.001E−05	1.704E−03
F			−8.064E−06	−6.692E−04
G				1.520E−04
H				−1.843E−05
I				9.114E−07
RMS fit error (μm)	0.03 ± 0.01	0.10 ± 0.2	0.26 ± 0.4	0.28 ± 0.4

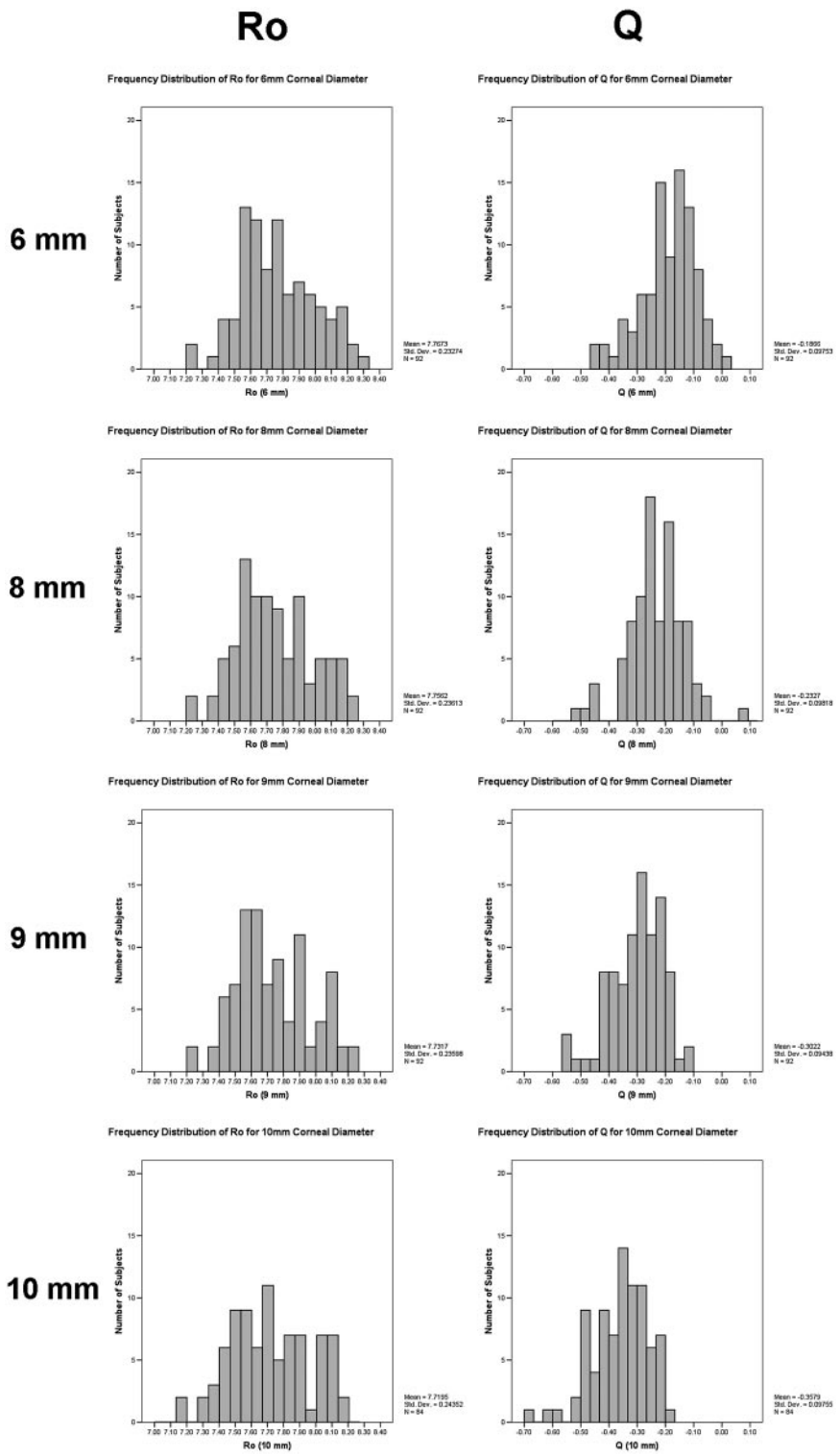

FIGURE 3. Frequency distributions for *Ro* and *Q* for 6-, 8-, 9-, and 10-mm corneal diameters.

are mutually exclusive (i.e., the inner annulus provides information about the central cornea only and the outer annulus provides information about the peripheral cornea only). The best fit spherocylinder was then calculated for each annulus of corneal axial power data and again broken down into the power vectors **M**, **J0**, and **J45**. For this analysis, only subjects with complete semimeridians of axial power data to 8-mm diameter were included.

We performed this analysis for annuli of 2-mm width and for those of 0.5-mm width. The 2-mm width analysis provides a measure of the central cornea from the inner annulus (from 0- to 4-mm diameter) and a measure of the peripheral cornea from the outer annulus (from 4- to 8-mm diameter). From this analysis we were able to classify broadly each subjects' central cornea as either type 1 (spherical central cornea with astigmatism < 0.75 D) or type 2 (astigmatic central cornea with astigmatism >0.75 D). The peripheral cornea was classified as type a (peripheral astigmatism stable, changing <0.25 D from the central cornea), type b (increasing peripheral astigmatism of ≥ 0.25 D), or type c (decreasing peripheral astigmatism of ≥ 0.25 D). Previous investigators have classified corneas according to central and peripheral astigmatism in a similar fashion.[3,4]

TABLE 2. Group Mean Conic Fit for the Steepest and Flattest Corneal Meridians

	Corneal Diameter					
	6 mm (n = 92)		8 mm (n = 86)		9 mm (n = 64)	
	Steep	Flat	Steep	Flat	Steep	Flat
Conic fit						
*R*o	7.69 ± 0.2	7.83 ± 0.2	7.69 ± 0.3	7.83 ± 0.2	7.68 ± 0.3	7.81 ± 0.2
Q	−0.21 ± 0.1	−0.17 ± 0.1	−0.27 ± 0.1	−0.23 ± 0.1	−0.32 ± 0.1	−0.30 ± 0.1
RMS fit error (μm)	1.99 ± 1.0	1.40 ± 0.7	5.39 ± 7.2	3.60 ± 1.8	15.59 ± 16.9	10.62 ± 5.8

The 0.5-mm analysis provides a higher resolution investigation of the changes in the corneal spherocylinder with increasing distance from corneal center. Figure 2 illustrates the corneal spherocylinder annulus analysis for one subject. To investigate changes in the annulus corneal spherocylinder with distance from corneal center, a repeated-measures ANOVA was used with one within-subject factor (corneal annulus diameter) and one between-subjects factor (central corneal type).

To provide a mathematical analysis of the corneal surface shape for each subject, Zernike polynomials were fit to the corneal height data using a least-squares fitting method.[36] Zernike polynomials up to and including the sixth radial order were fit to the corneal height data, for 6-, 8-, and 9-mm corneal diameters. The polynomials were expressed using the double indexed Optical Society of America (OSA) convention.[37] This fitting routine is also sensitive to any missing or invalid data. We therefore included only subjects with complete corneal height data to the 9-mm diameter in the analysis. A repeated-measures ANOVA was used with one within-subject factor (corneal diameter) to investigate changes in each of the higher-order Zernike polynomials (third-order and above) with increasing corneal diameter.

RESULTS

The map correlation and combination process provides a much larger corneal coverage than that given by standard topography maps alone. The average diameter of map for the standard corneal topography (central fixation) was 9.2 ± 0.3 mm in the horizontal dimension and 7.2 ± 0.7 mm in the vertical dimension. The average map diameter in the extended corneal topography maps was 11.4 ± 0.4 mm in the horizontal dimension and 9.8 ± 0.6 mm in the vertical dimension. This represents an increase in the horizontal and vertical map dimensions of 25% and 36%, respectively. The use of map combining therefore led to an approximate increase of 68% in corneal topography map area.

The average conic fit parameters (*R*o and *Q*), polynomial function, and RMS fit errors for the average corneal height data across all meridians are presented in Table 1. The average *R*o for a 6-mm corneal diameter was found to be 7.77 ± 0.2 mm and the average *Q* value was −0.19 ± 0.1. For a 10-mm corneal diameter, the average *R*o was 7.72 ± 0.2 and *Q* was −0.36 ± 0.2. This indicates an increase in the rate of corneal flattening for the peripheral cornea. Repeated-measures ANOVA revealed that both *R*o and *Q* changed significantly with increasing corneal diameter ($P < 0.0001$ for both *R*o and *Q*). The RMS fit error was found to increase dramatically for larger corneal diameters. For the conic fitting of the corneal data, the RMS fit error increased from a mean of 0.79 ± 0.4 μm for the 6-mm diameter to 21.18 ± 11.1 μm for the 10-mm corneal diameter. These fit errors highlight the inadequacy of the conic section to describe the peripheral cornea. To reduce the RMS fit error for larger corneal diameters, polynomial fitting to the data was required. For increasing corneal diameters, progressively higher-order fits were needed to fit the data reasonably (i.e., to reduce the RMS fit error). For a 6-mm corneal diameter, a fourth-order polynomial had an average RMS fit error of 0.03 ± 0.01 μm. For the 10-mm corneal diameter, a ninth-order polynomial fit gave an average RMS fit error of 0.28 ± 0.4 μm.

Figure 3 displays the frequency distribution for *R*o and *Q* for the different diameters tested and illustrates the relatively wide range of *R*o and *Q* in the population. The shift in *Q* to more a negative value for the larger corneal diameters is also highlighted in the frequency distribution plots.

The group mean *R*o and *Q* for the steepest and flattest corneal meridians are displayed in Table 2. The average *R*o along the steepest corneal meridian was found to be 7.69 ± 0.2 mm and was 7.83 ± 0.2 mm for the flattest meridian for a 6-mm diameter. The mean *Q* was −0.21 ± 0.1 along the steepest and −0.17 ± 0.1 along the flattest meridian for the 6-mm diameter. Both *R*o and *Q* were found to change significantly with increasing corneal diameter ($P < 0.001$ for *R*o and Q). This was a change similar to that found for the data averaged across all meridians. The repeated-measures ANOVA also revealed significant meridional variation in *R*o and *Q*. As would be expected, the *R*o was significantly different between the two meridians ($P < 0.0001$). The *Q* was also significantly different between the steepest and flattest meridians, with *Q* along the steepest meridian being significantly more negative ($P < 0.01$). This indicates that the steepest corneal meridian has a slightly greater rate of peripheral flattening. Both *R*o and *Q* showed significant diameter and meridian interactions ($P < 0.05$ for *R*o and *Q*).

TABLE 3. Group Mean Axial Power Corneal Spherocylinder for 6-, 7-, 8-, and 9-mm Corneal Diameters

	Corneal Diameter			
	6 mm (n = 78)	7 mm (n = 78)	8 mm (n = 78)	9 mm (n = 38)
M (D)	48.2 ± 1.5	48.1 ± 1.5	47.96 ± 1.5	47.28 ± 1.5
J0 (D)	0.32 ± 0.4	0.31 ± 0.4	0.30 ± 0.4	0.26 ± 0.3
J45 (D)	−0.05 ± 0.2	−0.04 ± 0.2	−0.03 ± 0.2	−0.05 ± 0.2

The power vectors **M** (best sphere), **J0** (astigmatism 90°/180°) and **J45** (astigmatism 45°/135°) are presented. Only those subjects with complete data to 8-mm diameter are presented.

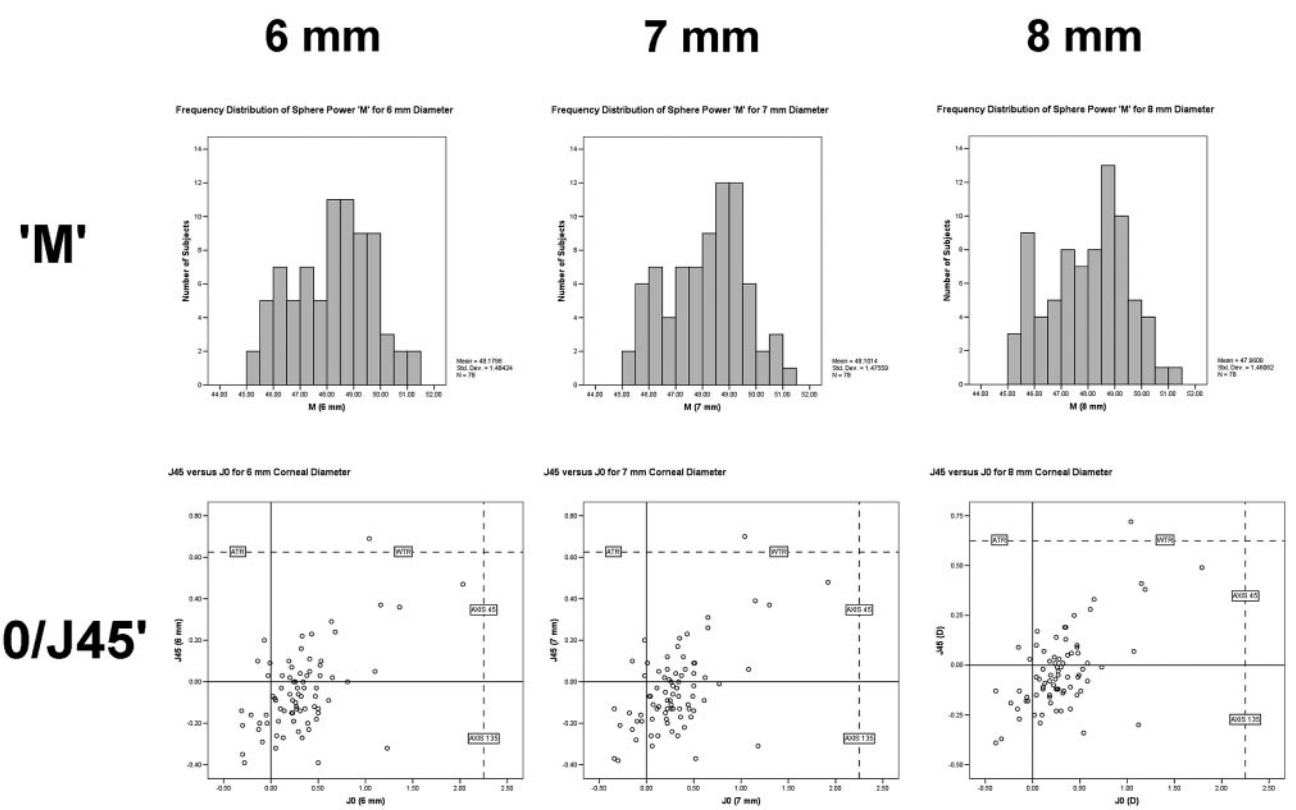

FIGURE 4. Frequency distribution for corneal power best sphere **M** for corneal diameters 6, 7, and 8 mm (*top*). Scatterplots of **J45** and **J0** for corneal axial power are displayed for 6-, 7-, and 8-mm corneal diameters (*bottom*).

The group mean best fit spherocylinder data for the axial power maps for 6-, 7-, 8-, and 9-mm corneal diameters are presented in Table 3. Figure 4 displays the frequency distribution for the sphere power **M** and scatter plots of astigmatism 90°/180° (**J0**) and astigmatism 45°/135° (**J45**) for the 6-, 7-, and 8-mm diameters. The average **M** was found to be 48.2 ± 1.5 D, **J0** was 0.32 ± 0.4 D, and **J45** was −0.05 ± 0.2 D for a 6-mm corneal diameter (this equates to an average corneal spherocylinder of 48.5/ −0.64 × 176). It is evident from the scatterplots in Figure 4 that most of the subjects exhibited positive **J0** and relatively small **J45**. In other words, most subjects exhibited a corneal cylinder axis relatively close to horizontal (i.e., with-the-rule [WTR] corneal astigmatism). With increasing corneal diameter the average **M**, **J0**, and **J45** all were reduced slightly in magnitude. These changes with increasing corneal diameter were found to be significant ($P < 0.0001$ for **M** and **J45** and $P < 0.01$ for **J0**). This indicates that the cornea flattens significantly in the periphery and exhibits a slight reduction in its toricity.

The 2-mm width corneal spherocylinder annulus analysis further highlights the changes occurring to the corneal spherocylinder in the peripheral cornea. For the central annulus (0- to 4-mm diameter annulus) the group mean **M** was 48.3 ± 1.5 D, **J0** was 0.32 ± 0.4 D, and **J45** was −0.07 ± 0.2 D (48.6/−0.7 × 174). For the peripheral annulus (4- to 8-mm diameter annulus) the group mean **M** was 47.6 ± 1.4 D, **J0** was 0.27 ± 0.3 D, and **J45** was −0.001 ± 0.2 D (47.9/−0.5 × 180).

The group mean best-fit corneal spherocylinder data for the 0.5-mm annulus analysis are presented in Table 4 and emphasize the changes occurring in the peripheral cornea. The average best sphere **M**, **J0**, and **J45** all decreased in magnitude with increasing annulus diameter. This manifests itself as a general flattening, a slight change in corneal cylinder axis and a slight reduction in corneal astigmatic power in the more peripheral cornea. Repeated-measures ANOVA revealed the changes occurring in **M**, **J0**, and **J45** with increasing annulus diameter to be highly significant ($P < 0.0001$ for **M** and **J45** and $P < 0.001$ for **J0**). Based on the classification according to central corneal type there were 42 subjects with a spherical central cornea (<0.75 D astigmatism) and 36 subjects with an astigmatic central cornea (>0.75 D astigmatism). A significant interaction was found to occur between corneal annulus diameter and

TABLE 4. Group Mean Axial Power Corneal Spherocylinder for 0.5-mm Annulus Data

	Outer Annulus Diameter (n = 78)						
	2 mm	**3 mm**	**4 mm**	**5 mm**	**6 mm**	**7 mm**	**8 mm**
M (D)	48.4 ± 1.5	48.3 ± 1.5	48.2 ± 1.5	48.0 ± 1.5	47.8 ± 1.5	47.6 ± 1.4	47.1 ± 1.4
J0 (D)	0.34 ± 0.4	0.32 ± 0.4	0.31 ± 0.4	0.31 ± 0.4	0.28 ± 0.4	0.24 ± 0.3	0.23 ± 0.3
J45 (D)	−0.09 ± 0.2	−0.06 ± 0.2	−0.05 ± 0.2	−0.03 ± 0.2	−0.001 ± 0.2	−0.003 ± 0.2	0.03 ± 0.2

The power vectors **M** (best sphere), **J0** (astigmatism 90°/180°) and **J45** (astigmatism 45°/135°) are presented, for outer annulus diameters from 2 mm to 8 mm. Only data from subjects with complete data out to 8 mm are presented.

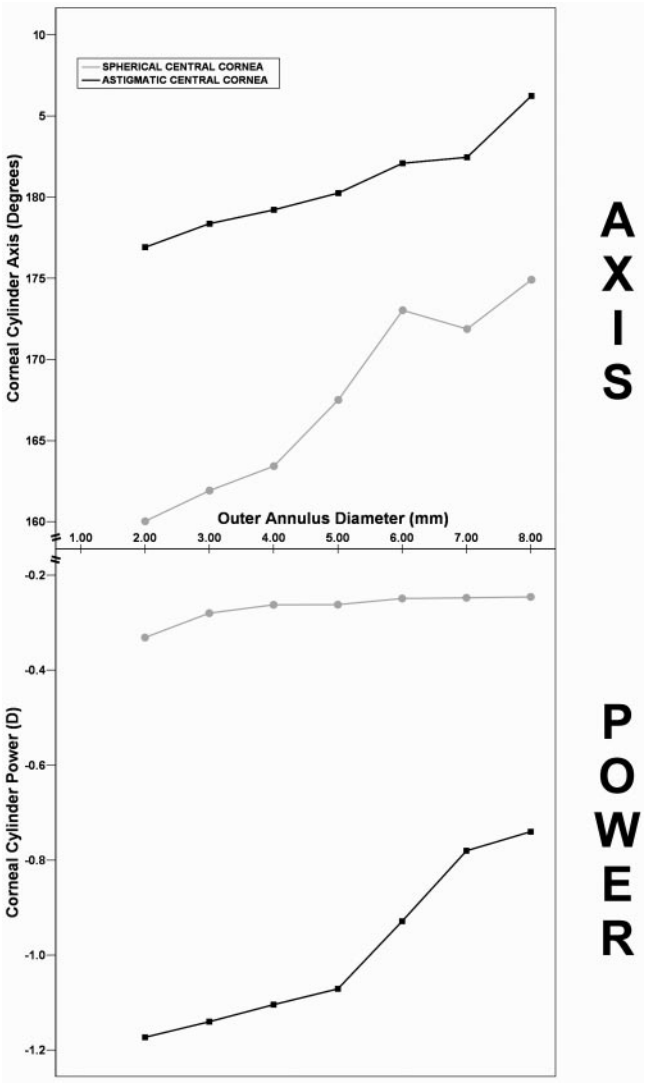

FIGURE 5. Corneal cylinder axis and cylinder power versus annulus diameter for the 0.5-mm annulus analysis.

central corneal type for the change in **J0** ($P = 0.0002$). This indicates that the reduction occurring in **J0** in the peripheral cornea was greater in subjects with greater central corneal astigmatism. Figure 5 shows the group mean corneal cylinder power and axis as a function of distance from corneal center for the 0.5-mm annulus analysis (data for both the central spherical and central astigmatic corneas are shown). It can be seen in this figure that the change in astigmatic power in the peripheral cornea was much greater in the subjects with astigmatic central corneas (astigmatic eyes showed an average reduction in cylinder from center to periphery of 0.43 D, whereas subjects with spherical central corneas showed only a 0.09-D reduction). The average change in cylinder axis in the peripheral cornea is similar between the two groups with both the astigmatic and spherical central cornea groups showing a slight anticlockwise shift in cylinder axis (right eye) with increasing distance from corneal center.

Although the annulus analysis data shows the average corneal toricity decreasing as a function of distance from corneal center, examination of individual subject data revealed several of different individual patterns of corneal topography. We classified each cornea based on the amount of central (type 1 or 2) and peripheral astigmatism (type a, b, c, or d). The different patterns of corneal topography found in the 78 subjects with complete data out to an 8-mm diameter in order of most common to least common were type 1, a (central spherical, periphery spherical, $n = 30$), type 2, c (central astigmatic, peripheral astigmatism decreasing, $n = 17$), type 2, a (central astigmatic, peripheral astigmatism stable, $n = 16$), type 1, c (central spherical, peripheral astigmatism decreasing, $n = 7$), type 1, b (central spherical, peripheral astigmatism increasing $n = 5$), and type 2, b (central astigmatic, peripheral astigmatism increasing $n = 3$). The most common peripheral corneal types were peripheral astigmatism stable ($n = 40$) and peripheral astigmatism decreasing ($n = 24$). Only 8 of the 78 subjects exhibited an increase in astigmatism in the peripheral cornea. Figure 6 shows examples of axial power maps and corneal cylinder power annulus maps for subjects with the different patterns of corneal astigmatism.

Correlation analysis was performed to investigate any association between the subjective refractive error best sphere and the corneal topography parameters. For the 8-mm corneal diameter analysis, the refractive error best sphere showed a weak but significant correlation with corneal best sphere **M** ($r = -0.266$, $P = 0.019$), indicating a tendency for the more myopic subjects to exhibit slightly steeper corneas. The best sphere refraction also showed a significant correlation with corneal **J0** ($r = -0.385$, $P = 0.001$) and corneal **J45** ($r = -0.284$, $P = 0.012$), indicating that the more myopic subjects also exhibit more astigmatic corneas (particularly with the rule astigmatism). The correlation coefficients and significances were also found to be similar for the 4-mm, 6-mm, and peripheral annulus corneal analysis diameters. No significant correlation was found between the asphericity parameter Q and best sphere refractive error in our population for any of the corneal analysis diameters tested ($r = 0.102$, $P = 0.335$ for the 8-mm corneal diameter).

Zernike polynomials up to and including the sixth radial order were fit to the corneal height data for 6-, 8-, and 9-mm diameters. Repeated measures ANOVA revealed several of the higher order Zernike coefficients to exhibit significant change with increasing corneal diameter. The Zernike polynomial coefficients Z_3^{-1} ($P = 0.001$), Z_3^1 ($P = 0.002$), Z_4^{-2} ($P = 0.009$), Z_4^0 ($P < 0.0001$), Z_4^4 ($P = 0.006$), and Z_6^0 ($P < 0.0001$) all showed highly significant change ($P < 0.01$) with increasing corneal diameter. Figure 7 shows the group mean third- and fourth-order corneal surface Zernike polynomial coefficient values (and Zernike term Z_6^0, as this was the only fifth- or sixth-order term exhibiting highly significant change) for the 6-, 8-, and 9-mm corneal diameters. It is evident in Figure 7 that the fourth-order term Z_4^0 was the higher-order coefficient of the largest magnitude and exhibited the largest change with increasing corneal diameter.

DISCUSSION

We have presented normative data across a range of parameters to describe the topography of the central and peripheral cornea in a large group of young, healthy, adult subjects. The use of a conic fit as an estimator of corneal shape has been performed in several studies of young adult subjects. This simple fitting method has the advantage that it defines the contour of the cornea with the use of only two parameters. A summary of studies into the average Ro and Q is presented in Table 5. It is clear from Table 5 that several different techniques have been used to measure the cornea in these studies. Despite this, our results (for the 6-mm corneal diameter) compare closely to these previous studies and correlate particularly closely with the two more recent studies that have also used a

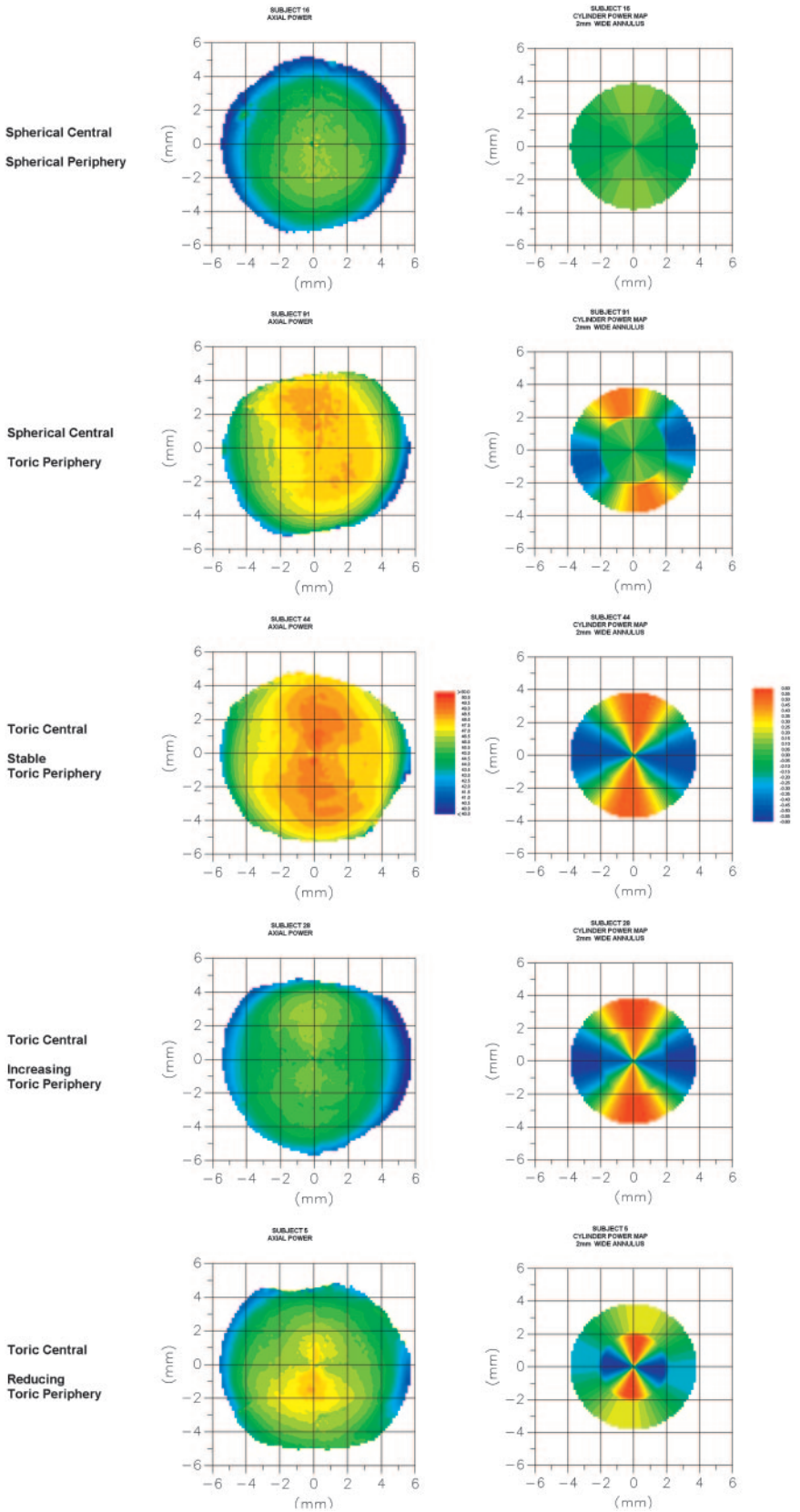

FIGURE 6. Examples of corneal classification based on central and peripheral toricity. *Left*: axial power maps. To highlight the changes in astigmatism, the maps on the *right* illustrate the cylinder power for the inner and outer annulus (i.e., the best sphere and all other surface irregularities have been removed from the data for each annulus).

videokeratoscope for corneal measurements. Corneal topography measures have been shown to exhibit several changes with subject age (with a shift toward a predominance of against-the-rule corneal astigmatism and slightly steeper, more irregular corneas found after the age of 50).[38,39] Differences in the age of subjects may therefore be a reason for some of the slight differences in results between our study, and previous studies. Our subjects were all young adults (age range, 18–35),

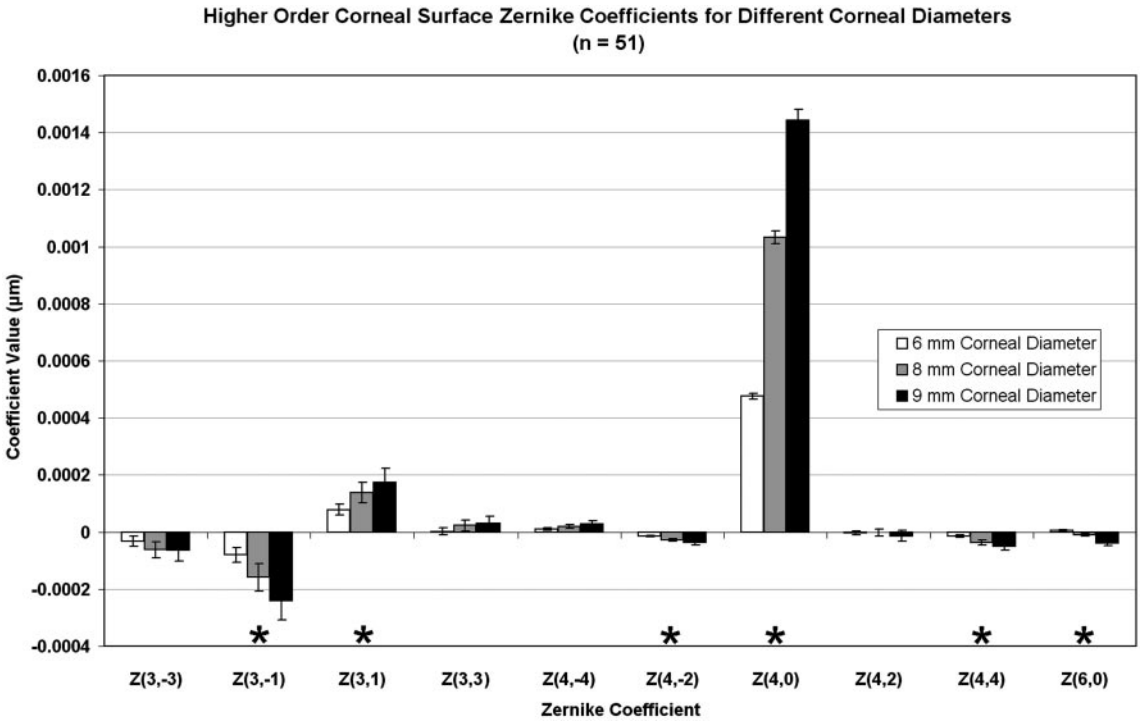

FIGURE 7. Third- and fourth-order Zernike polynomial coefficients (and term Z_0^0) for 6-, 8-, and 9-mm corneal diameters. *Coefficient exhibits highly significant change with increasing corneal diameter ($P < 0.01$). Error bars, SEM.

whereas most previous studies have investigated a wider range of ages, with many including subjects over the age of 50.

The average *Q* for the population in our study (and from previous studies) indicates that the average cornea has a prolate elliptical shape (i.e., steeper centrally and flattened in the periphery). Some investigators have stated that a small subset of normal subjects exhibit an oblate corneal shape (i.e., a cornea that is steeper in the periphery).[11–13] Eghbali et al.[13] found that 8 of their 41 subjects exhibited an oblate corneal profile. In our data, only one of our subjects exhibited a positive *Q* (oblate cornea) for the 6-mm measurement zone. For corneal diameters larger than 8 mm, all subjects were found to exhibit a prolate elliptical shape.

We found a small but significant meridional variation in the asphericity parameter Q, indicating that the steeper principal corneal meridian flattens at a slightly faster rate than the flattest meridian. Kiely et al.[11] also investigated meridional variation in the asphericity of the cornea and could find no specific trend for *Q* to differ from one meridian to the other. Other investigators have noted some small meridional variations to exist in corneal asphericity.[13,15] The difference that we found between the two principal corneal meridians was small in magnitude, but was highly statistically significant.

We have shown that the conic fit parameters *R*o and *Q* are highly dependent on the diameter of the cornea that is measured. With increasing corneal diameter *R*o reduces and *Q* becomes more negative (indicating an increased rate of flattening in the peripheral cornea). With increasing corneal diameter, the RMS fit error for the conic section also increases markedly. This indicates that although it is convenient and simple to understand, the conic section is a poor estimator of the peripheral cornea. To accurately specify the contour of the peripheral cornea, more complex fitting is required. We found that the use of a ninth-order polynomial function provided an excellent fit to the average corneal contour over a 10-mm diameter, producing an RMS fit error 75 times smaller than that given by the simple conic fitting.

The changes occurring in the contour of the cornea in the periphery will have little influence on foveal vision. Peripheral corneal changes, however, play a role in off-axis aberrations and vision. It is therefore possible that the changes occurring in the peripheral cornea are a part of the balancing of the peripheral refraction or aberrations. It is more likely though that the marked flattening of the cornea in the periphery occurs to produce a smooth transition from the cornea to the flatter scleral surface. The slight meridional variation in corneal asphericity (i.e., the steeper meridian's flattening more rapidly leading to a slight reduction in peripheral corneal toricity) may occur to minimize curvature change at the corneoscleral limbus, if we assume that the sclera is not toric. The corneal

TABLE 5. Summary of Studies of the Best-Fitting Conic Section to the Corneal Contour

Author	*n*	Age (y)	Method of Measurement	Corneal Diameter	Mean *R*o	Mean *Q*
Kiely et al.[11]	88	16–80	Photokeratoscope	6 mm	7.72 ± 0.3	−0.26 ± 0.2
Guillon et al.[12]	110	17–60	Photokeratoscope + keratometer	9 mm	7.78 ± 0.3	−0.15 ± 0.2
Eghbali et al.[13]	41	23–61	Videokeratoscope	6 mm	7.67 ± 0.2	−0.18 ± 0.2
Douthwaite et al.[15]	98	20–59	Videokeratoscope	6 mm	7.86 ± 0.2	−0.21 ± 0.1
Current study	92	18–35	Videokeratoscope	6 mm	7.77 ± 0.2	−0.19 ± 0.1

The average data across all meridians are presented. Gullion et al.[12] state that the photokeratoscope used can measure up to a 9-mm diameter, but the measured diameter may have been smaller. *n,* the total number of subjects tested in each study.

collagen orientation has been found to change in the limbal zone, becoming circumferentially oriented in the peripheral cornea.[40,41] This marked change in corneal stromal collagen orientation is the possible anatomic reason for the flattening and reduction in astigmatism found in the peripheral cornea.

We investigated the average corneal spherocylinder based on the corneal axial power data and found that most of our subjects exhibited some degree of with-the-rule (WTR) astigmatism (i.e., the steepest corneal meridian was oriented near vertical). This is consistent with many previous studies of corneal astigmatism in groups of young, healthy, adult subjects.[11,38,42–44] The best-fit corneal spherocylinder was also found to change significantly with increasing distance from corneal center. On average, the best fit sphere becomes flatter and the amount of corneal astigmatism reduces slightly in the peripheral cornea. This reduction in toricity of the peripheral cornea is consistent with the meridional variation found in the asphericity parameter *Q*. That is, as the steeper central meridian flattens at a faster rate in the periphery, then the degree of corneal astigmatism decreases in the corneal periphery.

Whereas, on average, the corneal astigmatism was found to decrease slightly in the periphery, several individual patterns of central and peripheral astigmatism were noted. The majority of subjects (59%) exhibited stable peripheral astigmatism or decreasing peripheral astigmatism (30%), with only 10% exhibiting an increase in corneal astigmatism in the corneal periphery. Guillon et al.[12] noted that most of their subjects displayed similar central and peripheral levels of astigmatism, but also noted some individual variations, with some subjects exhibiting a reduction or an increase in peripheral astigmatism. Reddy et al.[3] also classified their subjects' corneal topography based on central and peripheral corneal astigmatism. In contrast to our study, they found the most common form of astigmatism to be an increased or irregular astigmatism in the periphery, with stable or reducing corneal astigmatism found to be less common. This difference may be due to the subject selection procedures. In our study, we sought to examine the average corneal topography of normal healthy subjects, whereas the study by Reddy et al. involved subjects who were fitted with soft toric contact lenses. Thus, their population would be expected to have a much larger proportion of subjects with high degrees of corneal astigmatism (in fact, only 6% of their subjects had spherical central corneas). Their method for calculating peripheral astigmatism was also different to ours and was based on four corneal topography data points 3.5 mm from the center of the cornea.

The use of Zernike polynomials provides a mathematical description of the entire corneal surface (which does not require averaging across meridians of data as occurs for the conic and polynomial fitting to the average corneal contour). As we were interested in the shape of the cornea, we fit Zernike polynomials to the corneal surface shape, as opposed to deriving the corneal wavefront error (or corneal aberrations) from the corneal shape (which will give information on the cornea's optical effects). Particularly for the large corneal diameters that we have analyzed, it is not practical or realistic to consider the optical effects of the peripheral cornea. Figure 7 shows that the Zernike coefficients that made the greatest contribution to the higher order terms for all corneal diameters were the third-order Zernike terms (Z_3^{-3}, Z_3^{-1}, Z_3^1) and the fourth order term Z_4^0. The two terms displaying the most significant change with change in corneal diameter were the terms Z_4^0 and Z_6^0 (these corneal surface Zernike terms are analogous to the spherical aberration corneal wavefront error terms). The highly significant changes in these terms are due to the significant flattening occurring in the corneal periphery. Studies into corneal aberrations in normal healthy corneas have also found that the third-order terms and fourth-order spherical aberration term Z_4^0 to be the dominant higher-order aberration terms.[45–47] Increasing the corneal diameter over which the corneal aberrations are measured has also been found to cause a general increase in the higher order corneal aberrations, particularly for the spherical aberration and coma terms.[48–50]

The peripheral cornea does not contribute to foveal vision, but its shape is of great importance from an anatomic and mechanical point of view. It is of particular significance in the design and fitting of contact lenses. To characterize the shape of the normal central and peripheral cornea, we specifically excluded those subjects who had corneal disease or had undergone corneal surgery. Future research using these techniques to measure the peripheral cornea in subjects undergoing corneal refractive surgery or orthokeratology may improve our understanding of the changes to the peripheral cornea accompanying these procedures. Investigating the peripheral cornea in subjects with keratoconus or other corneal ectatic disorders may also provide further insight into the etiology of these corneal diseases.

In summary, we found the method of combining central and peripheral corneal topography data to provide a much larger area of corneal coverage than traditional videokeratoscopy. This method has allowed us to present a detailed analysis of the topography of the normal cornea to a large diameter. On average, the cornea flattens significantly and becomes slightly less astigmatic in the periphery. However, several different "patterns" of central and peripheral astigmatism were found in individual subjects. A conic section was found to be a poor estimator of the corneal shape for the peripheral cornea. Higher-order polynomial fits are necessary to describe the corneal contour adequately in the periphery.

Acknowledgments

The authors thank Brett Davis for assistance in the corneal spherocylinder analysis.

References

1. Schwiegerling J, Greivenkamp JE. Keratoconus detection based on videokeratoscopic height data. *Optom Vis Sci*. 1996;73:721–728.
2. Szczotka LB. Clinical evaluation of a topographically based contact lens fitting software. *Optom Vis Sci*. 1997;74:14–19.
3. Reddy T, Szczotka LB, Roberts C. Peripheral corneal contour measured by topography influences soft toric contact lens fitting success. *CLAO J*. 2000;26:180–185.
4. Szczotka LB, Roberts C, Herderick EE, Mahmoud A. Quantitative descriptors of corneal topography that influence soft toric contact lens fitting. *Cornea*. 2002;21:249–255.
5. Ambrosio R, Klyce SD, Wilson SE. Corneal topographic and pachymetric screening of keratorefractive patients. *J Refract Surg*. 2003; 19:24–29.
6. Varssano D, Kaiserman I, Hazarbassanov R. Topographic patterns in refractive surgery candidates. *Cornea*. 2004;23:602–607.
7. Alessio, Boscia F, La Tegola MG, Sborgia C. Topography-driven photorefractive keratectomy: results of corneal interactive programmed topographic ablation software. *Ophthalmology*. 2000; 107:1578–1587.
8. Knorz MC, Jendritza B. Topographically-guided laser in situ keratomileusis to treat corneal irregularities. *Ophthalmology*. 2000; 107:1138–1143.
9. Kanjani N, Jacob S, Agarwal A, et al. Wavefront- and topography-guided ablation in myopic eyes using Zyoptix. *J Cataract Refract Surg*. 2004;30:398–402.
10. Kymionis GD, Panagopoulou SI, Aslanides IM, Plainis S, Astyrakakis N, Pallikaris JG. Topographically supported customized ablation for the management of decentered laser in situ keratomileusis. *Am J Ophthalmol*. 2004;137:806–811.
11. Kiely PM, Smith G, Carney LG. The mean shape of the human cornea. *Opt Acta*. 1982;29:1027–1040.

12. Guillon M, Lydon DP, Wilson C. Corneal topography: a clinical model. *Ophthalmic Physiol Opt*. 1986;6:47–56.
13. Eghbali F, Yeung KK, Maloney RK. Topographic determination of corneal asphericity and its lack of effect on the refractive outcome of radial keratotomy. *Am J Ophthalmol*. 1995;119:275–280.
14. Carney LG, Mainstone JC, Henderson BA. Corneal topography and myopia: a cross sectional study. *Invest Ophthalmol Vis Sci*. 1997; 38:311–320.
15. Douthwaite WA, Hough T, Edwards K, Notay H. The EyeSys videokeratoscope assessment of apical radius and p-value in the normal human cornea. *Ophthalmic Physiol Opt*. 1999;19:467–474.
16. Keller P, van Saarloos P. Fourier transformation of corneal topography data. *Aust NZ J Ophthalmol*. 1997;25:S53–S55.
17. Schwiegerling J, Greivenkamp JE. Using corneal height maps and polynomial decomposition to determine corneal aberrations. *Optom Vis Sci*. 1997;74:906–916.
18. Guirao A, Artal P. Corneal wave aberration from videokeratography: accuracy and limitations of the procedure. *J Opt Soc Am A*. 2000;17:955–965.
19. Klein SA, Corzine J, Corbin JA, Wechsler S. Wide-angle cornea-sclera (ocular) topography. *Proc SPIE.* 2002;4611:149–158.
20. Mejia-Barbosa Y, Malacara-Hernandez D. A review of methods for measuring corneal topography. *Optom Vis Sci*. 2001;78:240–253.
21. Tang W, Collins MJ, Carney L, Davis B. The accuracy and precision performance of four videokeratoscopes in measuring test surfaces. *Optom Vis Sci*. 2000;77:483–491.
22. Cho P, Lam AKC, Mountford J, Ng L. The performance of four different corneal topographers on normal human corneas and its impact on orthokeratology lens fitting. *Optom Vis Sci*. 2002;79: 175–183.
23. Mandell RB. The cornea is not an ellipse (abstract). *Optom Vis Sci.* 1998;75(suppl 12):156.
24. Franklin RJ, Morelande MR, Iskander DRI, Collins MJ, Davis BA. Combining central and peripheral videokeratoscope maps to investigate total corneal topography. *Eye Contact Lens.* 2006;32:27–32.
25. Read SA, Collins MJ, Carney LG. The diurnal variation of corneal topography and aberrations. *Cornea*. 2005;24:678–687.
26. Buehren T, Collins MJ, Carney LG. Corneal aberrations and reading. *Optom Vis Sci*. 2003;80:159–166.
27. Fairmaid JA. The constancy of corneal curvature: an examination of corneal response to changes in accommodation and convergence. *Br J Physiol Opt*. 1959;16:2–23.
28. Lopping B, Weale RA. Changes in corneal curvature following ocular convergence. *Vision Res*. 1965;5:207–215.
29. Kwitko S, Suwasch MR, McDonnell PJ, Gritz DC, Moreira H, Evensen D. Effect of extraocular muscle surgery on corneal topography. *Arch Ophthalmol*. 1991;109:873–878.
30. Mandell RB. Apparent pupil displacement in videokeratography. *CLAO J*. 1994;20:123–127.
31. Mandell RB, Chiang CS, Klein SA. Location of the major corneal reference points. *Optom Vis Sci*. 1995;72:776–784.
32. Morelande MR, Iskander DR, Collins MJ, Franklin R. Automatic estimation of the corneal limbus in videokeratoscopy. *IEEE Trans Biomed Eng*. 2002;49:1617–1625.
33. Bennett AG. Aspherical and continuous curve contact lenses. *Optom Today*. 1988;28:11–14.
34. Maloney RK, Bogan SJ, Waring III GO. Determination of corneal image-forming properties from corneal topography. *Am J Ophthalmol*. 1993;115:31–41.
35. Thibos LN, Wheeler W, Horner D. Power vectors: an application of fourier analysis to the description and statistical analysis of refractive error. *Optom Vis Sci*. 1997;74:367–375.
36. Iskander DR, Collins MJ, Davis B. Optimal modelling of corneal surfaces with Zernike polynomials. *IEEE Trans Biomed Eng*. 2001; 48:87–95.
37. Thibos LN, Applegate RA, Schwiegerling JT, Webb R and VSIA Taskforce Members Standards for reporting the optical aberrations of eyes. *J Refract Surg.* 2002;18:S652–S660.
38. Hayashi K, Hayashi H, Hayashi F. Topographic analysis of the changes in corneal shape due to aging. *Cornea*. 1995;14:527–532.
39. Goto T, Klyce SD, Zheng X, Maeda N, Kuroda T, Ide C. Gender and age related differences in corneal topography. *Cornea*. 2001;20: 270–276.
40. Newton RH, Meek KM. Circumcorneal annulus of collagen fibrils in the human limbus. *Invest Ophthalmol Vis Sci*. 1998;39:1125–1134.
41. Meek KM, Boote C. The organization of collagen in the corneal stroma. *Exp Eye Res*. 2004;78:503–512.
42. Anstice J. Astigmatism: its components and their changes with age. *Am J Optom Arch Am Acad Optom*. 1971;48:1001–1006.
43. Baldwin WR, Mills D. A longitudinal study of corneal astigmatism and total astigmatism. *Am J Optom Physiol Opt*. 1981;58:206–211.
44. Grosvenor T, Ratnakaram R. Is the relation between keratometric astigmatism and refractive astigmatism linear? *Optom Vis Sci*. 1990;67:606–609.
45. Artal P, Guirao A, Berrio E, Williams DR. Compensation of corneal aberrations by the internal optics in the human eye. *J Vis*. 2001; 1:1–8.
46. Wang L Dai E Koch DD, Nathoo A. Optical aberrations of the human anterior cornea. *J Cataract Refract Surg*. 2003;29:1514–1521.
47. Kelly JE, Mihashi T, Howland HC. Compensation of corneal horizontal/vertical astigmatism, lateral coma and spherical aberration by internal optics of the eye. *J Vis*. 2004;4:262–271.
48. Oshika T, Klyce SD, Applegate RA, Howland HC, Danasoury MAE. Comparison of corneal wavefront aberrations after photorefractive keratectomy and laser in situ keratomileusis. *Am J Ophthalmol*. 1999;127:1–7.
49. Vinciguerra P, Camesasca FI, Calossi A. Statistical analysis of physiological aberrations of the cornea. *J Refract Surg*. 2003;19:S265–S269.
50. Nanba A, Amano S, Oshika T, et al. Corneal higher order wavefront aberrations after hyperopic Laser in situ Keratomileusis. *J Refract Surg*. 2005;21:46–51.